# Numerical Simulations of Altocumulus with a Cloud Resolving Model

*S. Liu and S. K. Krueger*
*Department of Meteorology*
*University of Utah*
*Salt Lake City, Utah*

## Introduction

Altocumulus and altostratus clouds together cover approximately 22% of the earth's surface (Warren et al. 1986; Warren 1988). They play an important role in the earth's energy budget through their effect on solar and infrared radiation. However, there has been little altocumulus cloud investigation by either modelers or observational programs.

Starr and Cox (SC) (1985a,b) simulated an altostratus case as part of the same study in which they modeled a thin layer of cirrus. Although this calculation was originally described as representing altostratus, it probably better represents altocumulus stratiformis (Houze 1993). In this paper, we simulate altocumulus cloud with a cloud resolving model (CRM). We simply describe the CRM first. We calculate the same middle-level cloud case as SC to compare our results with theirs. We will look at the role of cloud-scale processes in response to large-scale forcing. We will also discuss radiative effects by simulating diurnal and nocturnal cases. Finally, we discuss the utility of a 1D model by comparing 1D simulations and 2D simulations.

## Description of Model

The CRM is a 2D (x–z) numerical model. It is based on the anelastic set of equations. It includes third-moment turbulence closure, a turbulent scale condensation scheme, a bulk microphysics parameterization, and an advanced radiation code. The model is more fully described in Krueger (1988) and Xu and Krueger (1991). The radiative transfer parameterization used in the CRM is described in Fu (1991), Fu and Liou (1992), and Krueger et al. (1995). Neither ice-phase nor precipitation is considered in our simulations.

We also use a 1D version of the CRM in which the cloud-scale circulations and the small-scale turbulence are both parameterized. In such a 1D model, a major difficulty is determining the turbulent length scale, L(z). Bougeault and Andre (1986) proposed an "upward/downward free path" method to determine L(z), which is adopted in our 1D model.

The model domain we used for our numerical simulations is 6.4 km long and 8.9 km high. The horizontal grid interval is 100 m, while the vertical grid interval is 1 km from surface to 5 km, 500 m to 5.5 km, and 100 m from 5.5 km to 8.9 km. The time step is 10 seconds. The reference state is the U.S. Standard Atmosphere (USSA). The temperature and water vapor mixing ratio ($q_v$) from 5.5 km to 8.9 km is initialized the same as SC. At the levels outside this range, the temperature and $q_v$ are the same as the USSA. Random perturbations are used to initialize the potential temperature $\theta$ in the region between 7.2 and 7.5 km. The maximum initial magnitude of the perturbation is 0.1 K. The resulting surface flux is near zero. The ground temperature is fixed at the USSA surface air temperature.

## Simulations and Results

A series of numerical simulations, which are listed in Table 1, are performed by using the reference and initial conditions above. In Table 1, $w_0$ is the large-scale vertical velocity.

**Table 1**. Numerical simulations.

| Case | Dimension | Duration (h) | $w_o$ (cm/s) | Radiation |
|---|---|---|---|---|
| Q24 | 2D | 3 | 2 | nocturnal |
| Q05 | 2D | 6 | 0 | nocturnal |
| Q26[a] | 2D | 6 | 0 | nocturnal |
| Q27 | 2D | 3 | -2 | nocturnal |
| Q28[a] | 2D | 6 | 0 | dirunal |
| X25 | 1D | 6 | 0 | nocturnal |
| X26[b] | 1D | 6 | 0 | nocturnal |

(a) Continued from Q05.
(b) Continued from X25.

## Comparison to the Middle-Level Cloud Case of SC

We simulate a nocturnal case (Q24) which is the same as the case of SC (1985b) with $w_0 = 2$ cm/s. In Figure 1, the time-dependent behavior of the domain-averaged liquid water content ($\overline{\rho_0 l}$) is shown for SC and Q24. The agreement between SC and Q24 is good. In the first 25 minutes, the liquid water content increases quickly, and after 25 minutes, it increases slowly.

In Figure 2a and Figure 2b, profiles of horizontally averaged liquid water content ($\overline{\rho_0 l}$) are shown at various times during SC and Q24, separately. The agreement is also reasonable. In Q24, the cloud top and base height increase faster than those in SC. We compare the turbulent kinetic energy (TKE) in both cases. The TKE in Q24 is stronger. The maximum TKE (at 60 minute) is 0.145 J $kg^{-1}$ in SC and 0.177 in Q24. Considering our third-moment turbulence closure and SC's simple turbulence scheme, we believe that the TKE in Q24 is more realistic. The stronger TKE should be associated with stronger entrainment, so that the faster increase of cloud top height in Q24 is reasonable.

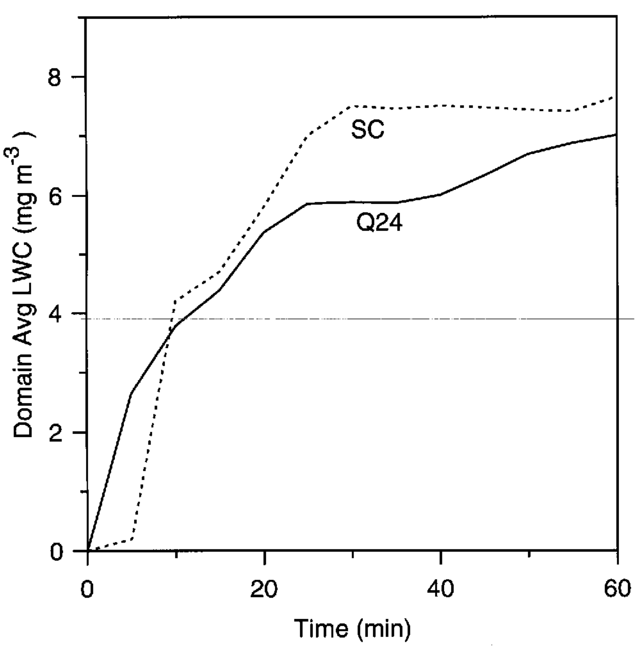


**Figure 1**. Time-dependent behavior of domain averaged liquid water content ($\overline{\rho_0 l}$) in SC and Q24.

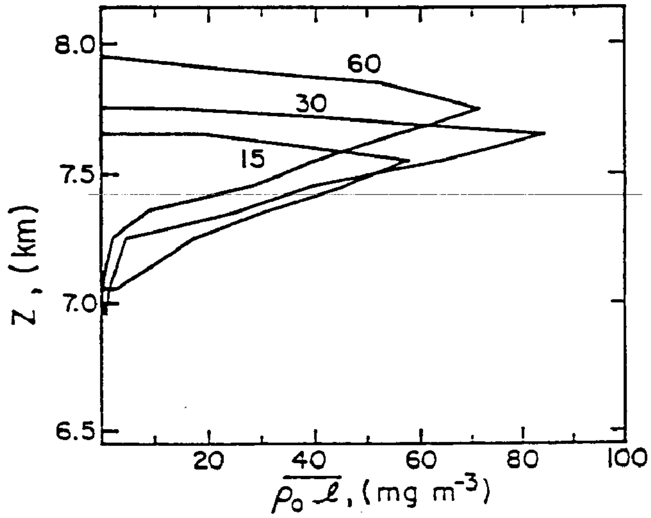


(a)

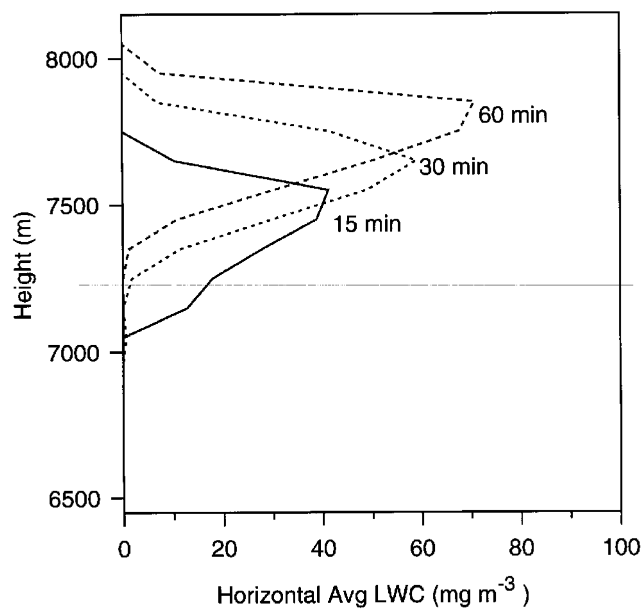


(b)

**Figure 2**. Vertical profile of horizontally averaged liquid water content ($\overline{\rho_0 l}$) at various times for (a) SC (from SC) and (b) Q24.

## Effect of Large-Scale Vertical Motion

In this section the effects of large-scale control via $w_0$ are briefly examined. In Figure 3, the temporal behavior of $\overline{\rho_0 l}$ is shown for three simulations (Q24, Q05, Q27) with

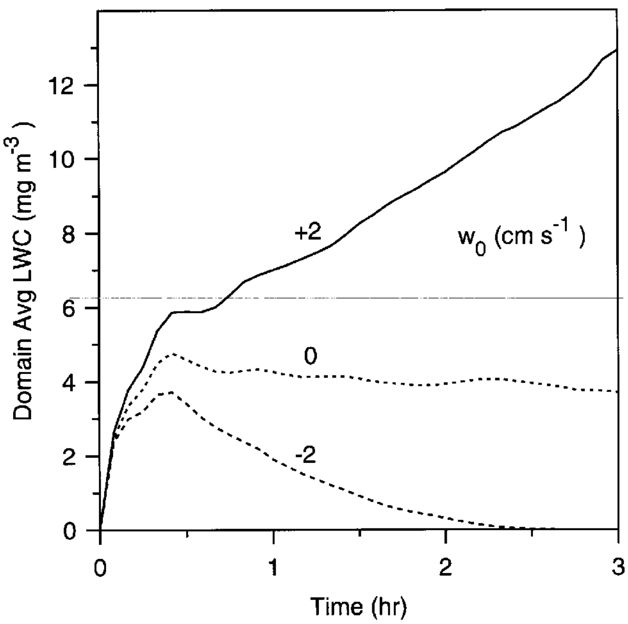


**Figure 3**. Time-dependent behavior of domain averaged liquid water content ($\overline{\rho_0 l}$) for different large-scale vertical velocities (Q24, Q05, and Q27).

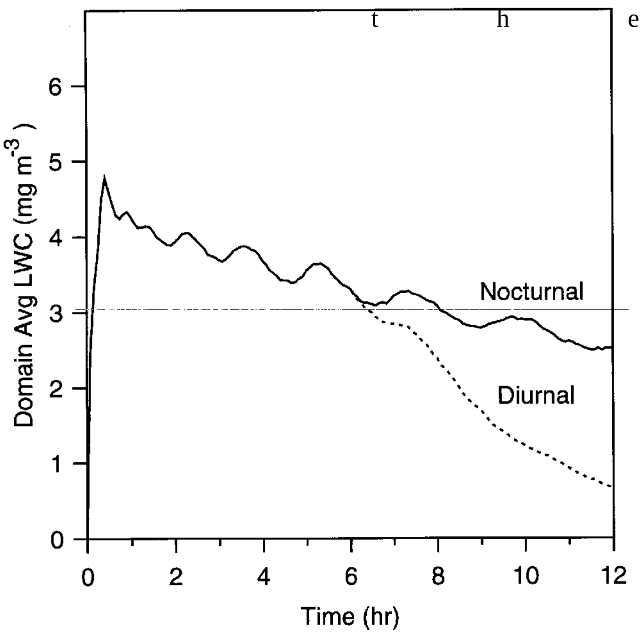


**Figure 4**. Time-dependent behavior of domain averaged liquid water content ($\overline{\rho_0 l}$) for a nocturnal case (Q05 + Q26) and a diurnal case (Q05 + Q28).

various specified values of $w_0$. Similar to the analysis of SC (1985b) for cirrus, each simulation may be also partitioned into three stages. During the initial stage, the response to the initial conditions dominates. This is followed by a transition or adjustment period. Then the solutions are dominated by the response to the continuing production of available water vapor and latent heat via $w_0$ as modulated by cloud-scale processes. With $w_0$ = 2 cm/s, $\overline{\rho_0 l}$ increases as the additional water vapor is available. With $w_0$ = −2 cm/s, $\overline{\rho_0 l}$ decreases to zero. It is interesting that $\overline{\rho_0 l}$ is almost steady when $w_0$ = 0. It shows that altocumulus may last a long time when there is no large-scale vertical motion.

## Effect of Radiation

We set $w_0$ = 0 for the discussion of radiative effects. Two cases are considered: one is a nocturnal case (Q05 + Q26), another is a diurnal case (Q05 + Q28). Q26 and Q28 are restarted from Q05 so that the simulated time period is from 6 to 12 hours. The date is July 15, and the latitude is 30 °N. In Figure 4, $\overline{\rho_0 l}$ is shown for each case. In Q28, $\overline{\rho_0 l}$ decreases sharply, which indicates that the cloud will disappear. In Q26, $\overline{\rho_0 l}$ decreases slowly, which indicates that the cloud can last for a longer time. In Figure 5, the total heating rates are shown at various times in Q26 and Q28. The cloud top region is a cooling region, and

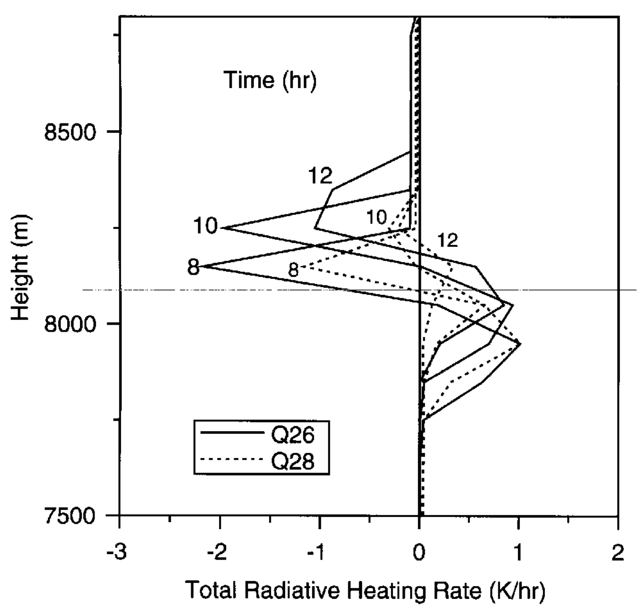


**Figure 5**. Total radiative heating rate profiles at various times for Q26 and Q28.

cloud base region is a heating region. In both cases the cooling rates decrease with time. However, in Q26 the cooling rates are very large. In Q28, it becomes very small at 10 and 12 hours. This shows that nighttime favors a longer lasting cloud.

## Comparison of 1D and 2D Simulations

In Figure 6, the temporal behavior of $\overline{\rho_0 l}$ is shown for a 1D simulation (X25 + X26) and a 2D simulation (Q05 + Q26). In the first hour, the agreement is good. After the first hour, $\overline{\rho_0 l}$ decreases slowly for the 2D case. For the 1D case it decreases quickly from 1 to 2 hours, then decreases slowly. The $\overline{\rho_0 l}$ for the 1D case is maximum about 20% less than that for the 2D case. In Figure 7, $\overline{\rho_0 l}$ is shown at various times in both the 1D and 2D cases. In both cases, the cloud ascends. The cloud ascends more slowly in the 1D case than in the 2D case, and the cloud is thinner in the 1D case. The maximum values of $\overline{\rho_0 l}$ are slightly larger in the 1D case.

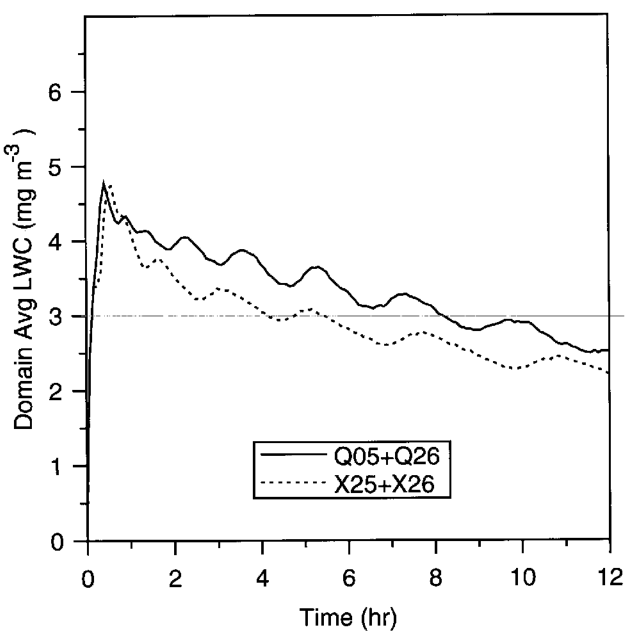


**Figure 6**. Time-dependent behavior of domain averaged liquid water content ($\overline{\rho_0 l}$) for a 2D simulation (Q05 + Q26) and a 1D simulation (X25 + X26).

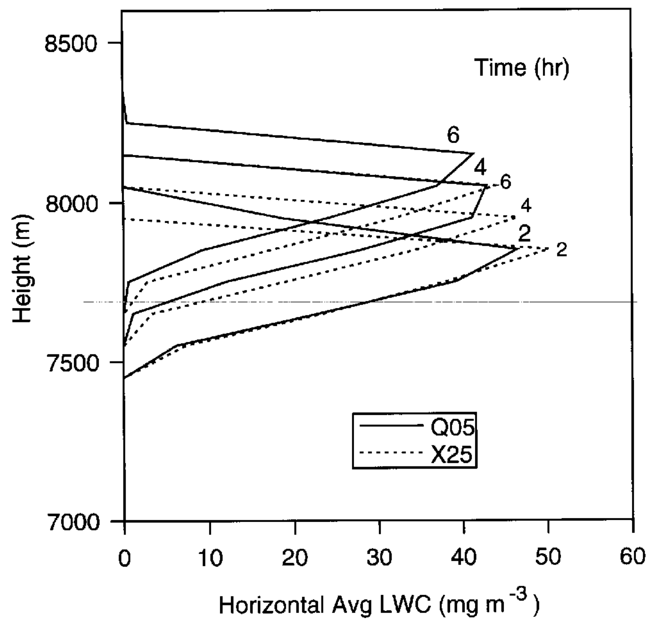


**Figure 7**. Vertical profiles of horizontally averaged liquid water content ($\overline{\rho_0 l}$) at various times for a 2D simulation (Q05) and a 1D simulation (X25).

## Summary

A series of numerical simulations is carried out with a 2D CRM and a 1D turbulence closure model. A good agreement between our 2D simulation and SC's altocumulus cloud case is achieved. After a middle-level cloud forms, weak large-scale vertical motion may allow for a long lifetime of the cloud. In nocturnal conditions, altocumulus can last longer than in diurnal conditions. The comparison of 1D and 2D simulations suggests that 1D simulations can portray the basic characteristics of altocumulus clouds.

## Acknowledgments

This research was supported by U.S. Department of Energy Grant DE-FG03-94ER61769. Computing assistance was provided by the National Center for Atmospheric Research Scientific Computing Division.

## References

Bougeault, P., and J.-C. Andre. 1986. On the stability of the third-order turbulence closure for the modeling of stratocumulus-topped boundary layer, *J. Atmos. Sci.*, **43**, 1574-1581.

Fu, Q. 1991. Parameterization of radiative processes in vertically nonhomogeneous multiple scattering atmospheres, Ph.D. dissertation, University of Utah, Salt Lake City, Utah.

Fu, Q, and, K. N. Liou. 1992. On the correlated k-distribution method for radiative transfer in nonhomogeneous atmospheres, *J. Atmos. Sci.*, **49**, 2139-2156.

Houze, R. A., Jr. 1993. *Cloud dynamics*. Academic Press.

Krueger, S. K. 1988. Numerical simulation of tropical cumulus clouds and their interaction with the subcloud layer, *J. Atmos. Sci.*, **45**, 2221-2200.

Krueger, S. K., G. T. Mclean, and Q. Fu. 1995. Numerical simulation of the stratus to cumulus transition in the subtropical marine boundary layer. Part 1: Boundary layer structure, *J. Atmos. Sci*, accepted.

Starr, D.O'C., and S. K. Cox. 1985a. Cirrus clouds. Part I: A cirrus cloud model, *J. Atmos. Sci.*, **42**, 2663-2681.

Starr, D.O'C., and S. K. Cox. 1985b. Cirrus clouds. Part II: Numerical experiments on the formation and maintenance of cirrus. *J. Atmos. Sci.*, **42**, 2682-2694.

Warren, S. G., C. J. Hahn, J. London, R. M. Chervin, and R. Jenne. 1986. Global distribution of total cloud cover and cloud type amount over land. NCAR Tech. Note TN-273 STR, 229 pp. National Center for Atmospheric Research, Boulder, Colorado.

Warren, S. G. 1988. *Global Distribution of Total Cloud Cover and Cloud Type Amount over the Ocean*. NCAR Technical Note TN-317 STR, 212 pp. National Center for Atmospheric Research, Boulder, Colorado.

Xu, K.-M., and S. K. Krueger. 1991. Evaluation of cloudiness parameterizations using a cumulus ensemble model, *Mon. Wea. Rev.*, **119**, 349-367.